Analysis of Backside Illuminated CMOS pixels' Quantum Efficiency under Ultraviolet Illumination

N. Fassi[1,2], J.-P. Carrère[1], E. Leon Perez[1], M. Estribeau[2], P. Magnan[2] and V.Goiffon[2]
1. STMicroelectronics, 850 rue Jean Monnet, 38926, Crolles, France
2. ISAE-SUPAERO, Université de Toulouse, 10 av Edouard Belin, 31055, Toulouse, France
Email : {nour.fassi, jean-pierre.carrere, edgar.leonperez}@st.com { magali.estribeau, pierre.magnan, vincent.goiffon}@ isae-supaero.fr

***Abstract*—The CMOS image sensor (CIS) market continues to grow and expand. One of the areas concerned by this expansion is UV applications. This work's main concern is to explain the performance of miniaturized backside-illuminated (BSI) CMOS pixels under UV light in the range of 200 nm to 400 nm. A previous study showed a quantum efficiency (QE) loss of nearly 50% between 400 nm (blue light) and 200 nm (UV-C).**

This study relies on optical and electrical simulations to understand the QE drop's causes for n-type photogate pixels. Electrical simulations show that the electric field was high at the interface, allowing the photogenerated electrons to drift rapidly. Therefore, the hypothesis that links the QE loss to a recombination rate increase at the interface seems to fade, leading to new recombination mechanisms to investigate.

Keywords—ultraviolet, backside illuminated pixels, CMOS image sensors, quantum efficiency, interface defects, antireflective coatings.

I. INTRODUCTION

Ultraviolet (UV) detection [10 nm, 400 nm], is becoming more prominent in different areas, including forensics and environmental hazard detection [1]. However, to be able to detect UV, we are facing several challenges. First, according to Beer-Lambert law, 90% of UV light with a wavelength shorter than 300 nm is absorbed in the first 6 nm of Si (Fig. 1.)

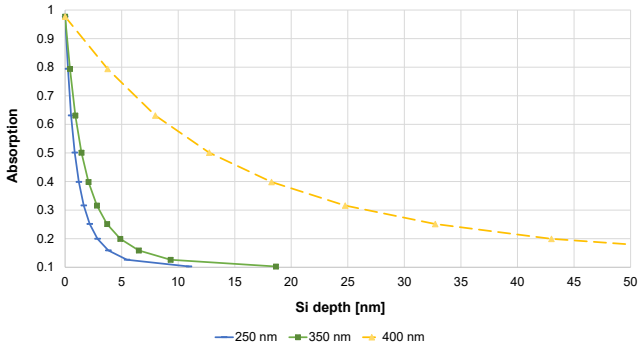

Fig. 1. UV light absorption in Si, according to Beer-lambert law

Another difficulty is the important role of Si/ SiO_2 interface defects [2] [3] on charge collection efficiency.

The current work focuses on the absorption of Si and the influence of interface recombination on QE for UV wavelengths. As the wavelength becomes shorter, there may be a significant impact due to interface defects, which can increase with photon energy.

For this purpose, electro-optical simulations in visible light (VIS) and UV were carried out in TCAD environment.

II. EXPERIMENTAL

The QE under UV of a p-type and a n-type BSI photogate (PG) pixel (Fig. 2.a&b) was measured.

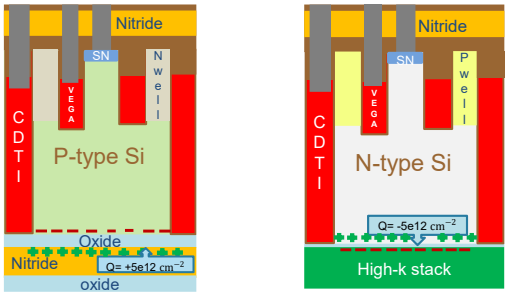

(a) (b)

Fig. 2. Schematic cross section of a p-type PG (a) and an n-type PG (b), adapted from [4]

The reason for that choice is that the photogate has the possibility of being fully depleted. In theory, the PG can overcome this limited absorption depth of Si under UV without having to modify the Si epitaxy process to make it thinner.

The operating principle of the photogate pixel is simple: capacitive deep trench isolation (CDTI) offers fully depleted Si for carriers' storage and dark current reduction. Also, PG uses epitaxial Si as an active layer, and its process does not involve any implantation, avoiding any interaction with process flow-related steps. On top of the device, front-side vertical Shallow Trench Transfer Gate and Planar Read-Out transistor are implemented, and the well region resulting from the transistor realization works as the top PG pinning layer. On the backside, the silicon surface passivation layer, also known as antireflective coating (ARC) is deposited, depending on the Si doping (n or p) [4].

Both investigated photogates give us the opportunity to have a closer look at two ARC stacks, namely high-k and oxide-nitride-oxide (ONO). Passivation of those pixels is ensured by inherent material fixed charges: for p-type pixels, a positively charged ONO stack, for which an electron-filled interface is needed, and a negative charged high-k stack (with high dielectric constant materials), for n-type pixels [5].

It is worth stating that measurements were carried out on pixels without micro-lenses.

Next, quantum efficiency measurements were carried out using a monochromator and a xenon lamp to measure QE down to 200 nm with a sampling step of 10 nm, at 40°C, with a f number of f/2 and a slit aperture of 15 nm [6].

Electro-optical simulations are performed using 3D TCAD tools from Synopsis.

III. RESULTS

A. Optical measurements

Although the photogate pixel is optimized for visible light, it shows a quite good QE response in the UV, comparable to the literature. However, both types of photogates show an approximately 50% decrease while the wavelength varies from 400 nm to 300 nm, as shown in (Fig. 3.)

To understand this trend, investigations should focus on whether this is due to phenomena related to the silicon or silicon oxide interface or to the anti-reflective coatings (ARC) absorption, the ARC being a back interface passivation, preventing recombination, depends on the nature of the silicon interface.

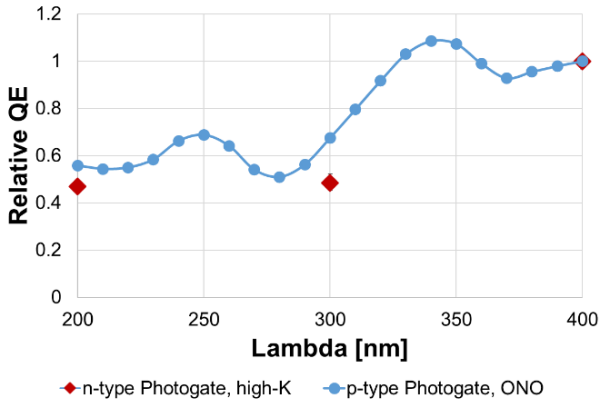

Fig. 3. Relative QE of n-type and p-type photogates under UV normalized at 400 nm

IV. SIMULATIONS

A. Electrical simulations

The electrostatic comparison of n-type and p-type PG is presented in (Fig. 4), where the potential map looks rather similar.

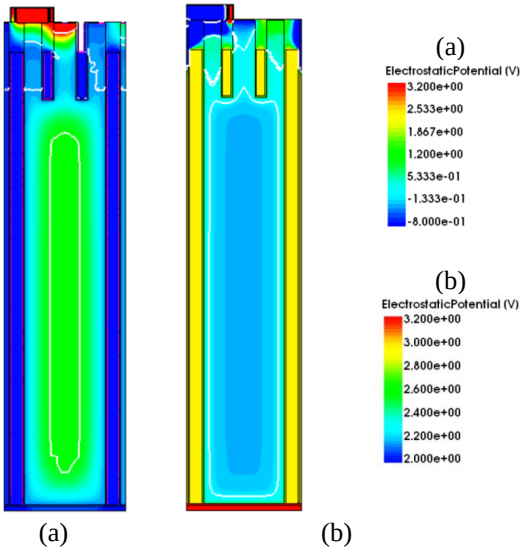

Fig. 4. Cross section showing electrostatic potential of n-type (a) and p-type (b) photogates

For the next simulation, focus is on the n-type PG because its ARC stack's inherent charge induces a higher electric field (as visible in Fig. 5). We can also notice that for the same fixed charge, the interface's electric field is much higher for n-type pixels than for p-type ones.

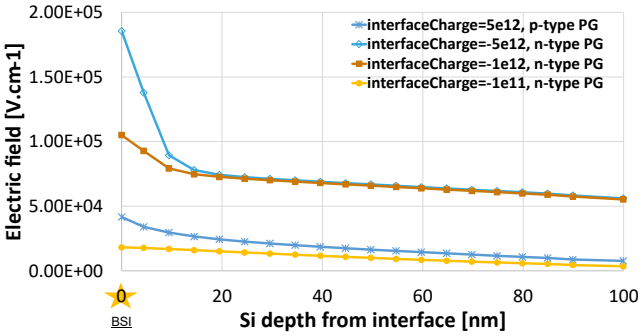

Fig. 5. The first 0.1 µm of Si from the backside, to see the impact of different interfaces or interface's charge on electric field.

Indeed, the interface charge does not influence much the deep potential profile (see Fig. 6), but it brings out a little more electric field in the backside (as shown in Fig. 5).

The next electrical behavior simulation is of an n-type PG pixel (Fig. 2.b), to study the behavior of the photogenerated charges close to the backside interface.

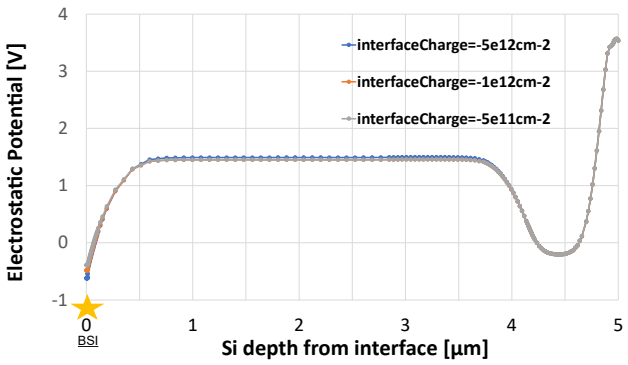

Fig. 6. Impact of the backside interface charges on the electrostatic potential of a n-type photogate pixel.

B. Illumination simulation

Illuminations under different wavelengths have been simulated using the 3D TCAD tools and its optical generation function, as (Fig. 7) illustrates. For each wavelength, the number of incident photons has been kept constant, corresponding to the experimental conditions of the QE measurement. The quantum yield (QY) of the pixel has next been calculated as the ratio of collected electrons over the number of optically photogenerated electrons inside the pixel silicon volume.

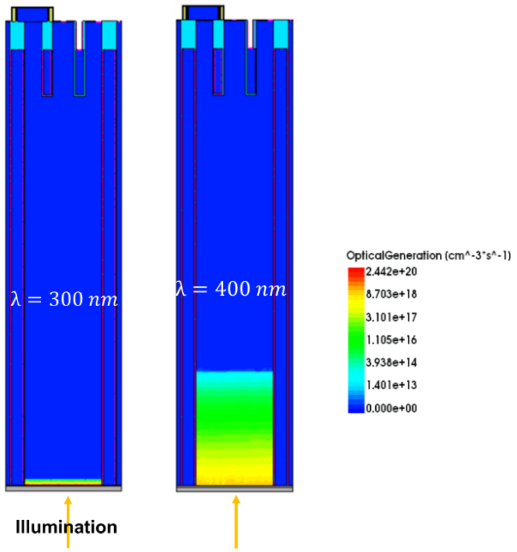

Fig. 7. Cross section of optical generation simulation in a n-type PG, illuminated from backside at (a) $\lambda = 300\ nm$ and (b) $\lambda = 400\ nm$

The simulations solve Poisson and continuity equations for drift-diffusion of carriers and Shockley-Read-Hall (SRH) recombination, which uses the Scharfetter model. Trap density levels within silicon were introduced in a second step.

Table I summarizes the QY simulation checks without trap: we verify that the QY is about 100%, and hence all the photogenerated charges are collected.

Fig. 8 shows the photogenerated electrons and their distribution among the silicon depths, for 200nm, 300 nm, and 400 nm UV illuminations. Total generated charges were normalized to 100 electrons for the whole pixel.

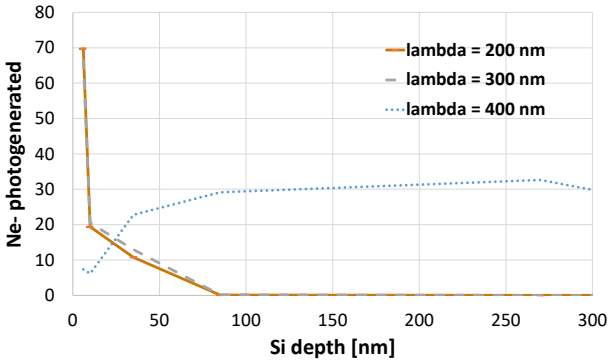

Fig. 8. Photogenerated electrons in relative values, depending on the Si depth in the pixel and the illumination wavelength, no traps added to the simulation.

We can observe that, indeed, most electrons are generated in the first few nanometers of bulk silicon, especially at wavelengths shorter than 300 nm. For 400nm wavelength illumination, the electrons are generated deeper, between 100 nm and 300 nm from the interface.

Once collected by the photogate electric field, the photogenerated electrons are located in the well of the center of the structure, as shown by the electrostatic potential in Fig. 6.

C. *Illumination simulation with interface traps*

Next, traps have been introduced on the backside interface to study their impact on the photogenerated charges. The trap's characteristics are donor in our case, and the cross section is about 5.10^{-13} cm^{-2} in this simulation; the traps' density has been modulated.

TABLE I SIMULATED QUANTUM YIELD OF THE PIXEL, WITH AND WITHOUT BACKSIDE INTERFACE TRAPS

λ [nm]	Trap type	QY
400	No traps	100%
	Traps, donor Dit = 2e11 cm^{-2}	~100%
	Traps, donor Dit = 2e12 cm^{-2}	~100 %
300	No traps	100%
	Traps, donor Dit = 2e11 cm^{-2}	~100%
	Traps, donor Dit = 2e12 cm^{-2}	~100%
200	No traps	100%
	Traps, donor Dit = 2e11 cm^{-2}	~100%
	Traps, donor Dit = 2e12 cm^{-2}	~100%

We observe in Table 1 that the introduction of the backside interface traps has no significant impact on the pixel's internal Quantum efficiency. This suggests that the recombination effect of the photogenerated electrons on the backside interface traps does not explain the QE decrease from 400 to 200nm.

D. *Optical simulations*

The ARC stacks are optimized for visible applications. Fig. 9 shows refraction simulations of the two ARC stacks used in the two PG pixels: they both have good antireflection properties even in the UV spectrum.

However, the transmittivity simulation result implies that the stack absorption under UV could also impact the transmission.

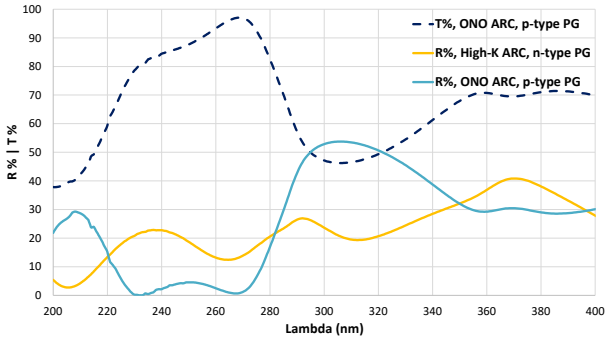

Fig. 9. p-type and n-type PG ARC reflectivity simulations under UV wavelengths, and transmission simulation of p-type PG ARC stack

V. DISCUSSION

As observed from the measurements and optical simulations, ARC stacks can indeed modulate the QE appearance.

Considering the P-Type PG, the simulated transmission drops from 70% to 40% between 400nm and 200nm; this is indeed a ratio comparable to the one observed during the measurements. However, the shape of the measured QE does not look like the transmission, this may perhaps be explained by the use of a 1-D optical simulation. Additional work, including ellipsometry measurements and simulations, will help verify this assumption as well as to get more information about N-Type PG stack transmission.

What follows is an explanation for the excellent electrical quantum yield of the pixel. We must take into consideration that the interface electric field can help electrons drift quicker to the depletion zone or even to the collection zone. Fig. 6

shows that the ARC fixed charges account for a strong interface electric field, which can reach 1.8 10^5 V.cm^{-1}, a value stronger than some widely used values observed for different dopant distributions [7]. With such an electric field, the photogenerated electrons drift velocity µ.E can reach high values close to the silicon saturation v_s about 10^7 cm/s.

With this drift velocity, the time spent at the interface can now be estimated by the electrons generated in the first ten nanometers, which will be less than 1ps, not allowing much trapping impact probability to happen. Especially if we consider that the surface recombination velocity is between 200 and 300 cm.s^{-1} [8] which leads to a recombination time way bigger than the speed at which the interface is crossed.

Finally, the backside drift velocity in the pixel seems to be optimal to collect UV photogenerated carriers at the interface, preventing the sensitivity loss due to carriers' recombination, as illustrated in Fig. 10.

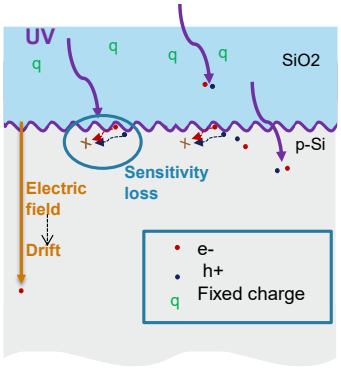

Fig. 4. Schematic illustration of a pixel's cross section with UV-induced oxide charging effects, inspired from [2]

Many plausible explanations for QE loss are discussed below. First, the other pixel interface may have a role in the carriers' recombination effect, like the sidewall interface of the CDTI trench. Indeed, carriers generated very close to the backside interface may show more sensitivity during their transport to SRH recombination occurring at the sidewall interface traps.

Next, other recombination mechanisms may occur with such a high carrier density, like band-to-band recombination, where energy is exchanged in a radiative or Auger process.

This very high density of carriers at the interface is most likely a factor that increases the capture probability and so decreases the recombination lifetime, as demonstrated by (1), A, B & C being defined in [9] n_d is the defect density and $n_{s,s',\alpha}$ the electron density.

$$R_{ec} \approx \frac{2\pi}{\hbar} n_d \times A \times \left[n_{s,s',\alpha} + B\right] \times C \qquad (1)$$

The ARC absorption has a key role too; it does prevent photons from reaching silicon.

Hence, after transmitting only a percentage of the photons, depending on the nature of the ARC, a good part of the photogenerated electrons probably drift away thanks to the strong electric field at the interface, but part of them remains and suffers the effects of recombination at the interface, which degrades the QE.

These stated effects were not considered in the presented simulations and will be investigated in further work. The optical behavior of the antireflective stack will also be compared with 3D Lumerical simulations.

VI. CONCLUSION

Quantum efficiency (QE) on different BSI pixels have been measured under UV. Despite a quite good response in UV, a loss at shorter wavelengths was noticed, and the inducing phenomena were discussed.

ARC stack transmission seems to modulate the QE, but the simulated transmission shape is not really in accordance with the measured QE shape for the P-type PG pixel. Additional ellipsometry measurements and Lumerical simulations must be conducted on both P-Type and N-type pixels to understand their behavior.

Backside traps SRH recombination does not seem either to be the first cause of this QE loss, due to the high electric field at this interface. Finally, the main causes of the QE loss at short wavelengths are most probably recombination enhanced by the very high density of photogenerated carriers at the interface, or recombination during the carriers' transport.

ACKNOWLEDGMENT

Special thanks and gratitude to the electro optical characterization sensors (EOCS) team of STmicroelectronics, Crolles, for their time and advice, to Pascal Fonteneau and Olivier Marcelot for their support and guidance in TCAD.

REFERENCES

[1] Okino, T., Yamahira, S., Yamada, S., Hirose, Y., Odagawa, A., Kato, Y., & Tanaka, T. (2018). A real-time ultraviolet radiation imaging system using an organic photoconductive image sensor. Sensors, 18(1), 314.

[2] Nakazawa, T., Kuroda, R., Koda, Y., & Sugawa, S. (2012, February). Photodiode dopant structure with atomically flat Si surface for high-sensitivity and stability to UV light. In Sensors, Cameras, and Systems for Industrial and Scientific Applications XIII (Vol. 8298, pp. 186-193). SPIE.

[3] LI, Flora et NATHAN, Arokia. CCD image sensors in deep-ultraviolet: degradation behavior and damage mechanisms. Springer Science & Business Media, 2005.

[4] Roy F, Suler A, Dalleau T, Duru R, Benoit D, Arnaud J, Cazaux Y, Chaton C, Montes L, Morfouli P, Lu G-N. Fully Depleted, Trench-Pinned Photo Gate for CMOS Image Sensor Applications. Sensors. 2020; 20(3):727. https://doi.org/10.3390/s20030727

[5] SACCHETTINI, Y., CARRÈRE, J.-P., DOYEN, C., et al. A highly reliable back side illuminated pixel against plasma induced damage. In : 2019 IEEE International Electron Devices Meeting (IEDM). IEEE, 2019. p. 16.5. 1-16.5. 4.

[6] Fassi, N, Carrère, JP., Estribeau, M., Goiffon, Vincent. (2023, January). Quantum efficiency of various miniaturized backside illuminated CMOS pixels under ultraviolet illumination. In Proc. IS&T Electronic Imaging.

[7] Hoenk, M. E., Jones, T. J., Dickie, M. R., Greer, F., Cunningham, T. J., Blazejewski, E. R., & Nikzad, S. (2009). Delta-doped back-illuminated CMOS imaging arrays: progress and prospects. Infrared Systems and Photoelectronic Technology IV, 7419, 187-201.

[8] Eades, W. D., & Swanson, R. M. (1985). Calculation of surface generation and recombination velocities at the Si-SiO2 interface. Journal of applied Physics, 58(11), 4267-4276.s, W. D., & Swanson, R. M. (1985). Journal of applied Physics, 58(11), 4267-4276.

[9] Wang, H., Strait, J. H., Zhang, C., Chan, W., Manolatou, C., Tiwari, S., & Rana, F. (2015). Fast exciton annihilation by capture of electrons or holes by defects via Auger scattering in monolayer metal dichalcogenides. Physical Review B, 91(16), 165411.